

NACA RM A52F17

SEP 19 1952

UNCLASSIFIED



RESEARCH MEMORANDUM

INVESTIGATION OF AN NACA SUBMERGED INLET

AT MACH NUMBERS FROM 1.17 TO 1.99

By Warren E. Anderson and Alson C. Frazer

Ames Aeronautical Laboratory
Moffett Field, Calif.

CLASSIFICATION CANCELLED

Authority *NACA R 7-2748* Date *10/12/54*

By *WETA 10/2/54* See _____

CLASSIFIED DOCUMENT

This material contains information affecting the National Defense of the United States within the meaning of the espionage laws, Title 18, U.S.C., Secs. 793 and 794, the transmission or revelation of which in any manner to an unauthorized person is prohibited by law.

NATIONAL ADVISORY COMMITTEE FOR AERONAUTICS

WASHINGTON
September 15, 1952

UNCLASSIFIED

NACA LIBRARY

~~CONFIDENTIAL~~

LANGLEY AERONAUTICAL LABORATORY
Langley Field, Va.

~~CONFIDENTIAL~~

UNCLASSIFIED

NATIONAL ADVISORY COMMITTEE FOR AERONAUTICS

RESEARCH MEMORANDUM

INVESTIGATION OF AN NACA SUBMERGED INLET

AT MACH NUMBERS FROM 1.17 TO 1.99

By Warren E. Anderson and Alson C. Frazer

SUMMARY

An investigation was conducted with an NACA submerged inlet at Mach numbers from 1.17 to 1.99. Total-pressure ratio, mass-flow ratio, and static pressure distribution along the ramp and main body were obtained at angles of attack of 0° and 6° for a side inlet location. The effects of both a round and a sharp lip profile were investigated.


The test results showed that the maximum total-pressure ratio attainable with the submerged inlet decreased from 0.83 at a Mach number of 1.17 to 0.52 at a Mach number of 1.99. A comparison at Mach numbers up to 1.26 showed lip shape had no significant effect on pressure recovery, but the sharp lip made it possible to obtain slightly higher mass-flow ratios.

Evaluation of submerged inlet performance at a Mach number of 1.36 showed that the net thrust coefficient was 87 percent of that for a normal-shock-type scoop inlet at the design mass-flow ratios. Increasing the Mach number to 1.51 reduced this value to 81 percent.

INTRODUCTION

Supersonic aircraft in many cases will be required to fly for extended periods of time at transonic and subsonic speeds. The air induction system for a jet-powered supersonic aircraft, therefore, will usually be a compromise between optimum designs for subsonic, transonic, and supersonic operating conditions. A practical inlet design must not only give high performance at design conditions, but must also satisfy requirements dictated by the off-design operating schedule of the aircraft.

The NACA submerged inlet was originally designed to operate at subsonic speeds (references 1 and 2) and has been shown to operate efficiently



UNCLASSIFIED

at high subsonic and transonic speeds (references 3 to 6). These results indicate that the submerged inlet may be applicable in the design of supersonic aircraft. The purpose of the present investigation was to measure the performance of a submerged inlet at supersonic speeds and to compare its performance with that of a normal-shock-type scoop inlet. This latter inlet is believed to have good performance in the lower range of supersonic Mach numbers where the submerged inlet also could be expected to operate satisfactorily.

NOTATION

- A cross-section area of duct or stream tube, square feet
- A_x component of area normal to free-stream direction, square feet
- C_{D_E} external drag coefficient of air induction system $\left(\frac{D_E}{q_o A_o} \right)$
- C_{D_S} scoop incremental drag coefficient $\left(\frac{D_S}{q_o A_o} \right)$
- C_{F_1} internal thrust coefficient $\left(\frac{F_1}{q_o A_o} \right)$
- C_{F_N} inlet net thrust coefficient $\left(\frac{F_N}{q_o A_o} \right)$
- $\left(C_{F_N} \right)_P$ inlet net thrust coefficient referred to engine frontal area $\left(\frac{F_N}{q_o S_P} \right)$
- D_E external drag force due to the air-induction system $(D_{B+S} - D_B + D_S)$, pounds
- D_{B+S} pressure and friction drag forces acting on the external surface of the combined basic body and air-induction system, pounds
- D_B pressure and friction drag forces acting on the basic body shape (fuselage) without an air inlet, pounds
- D_S scoop incremental drag due to a change in total momentum of the entering stream tube from free stream to the entrance, pounds

F_i	internal thrust force due to a change in total momentum of the entering flow from free stream to the exit where static pressure is assumed equal to free-stream static pressure, pounds
F_N	inlet net thrust ($F_i - D_E$), pounds
H	total pressure, pounds per square foot
L	forebody length, feet
M	Mach number
m	mass flow, slugs per second
$\frac{m_i}{m_o}$	mass-flow ratio $\left(\frac{\rho_i V_i A_i}{\rho_o V_o A_o}\right)$
P	static pressure coefficient $\left(\frac{P_i - P_o}{q_o}\right)$
p	static pressure, pounds per square foot
q	dynamic pressure $\left(\frac{1}{2} \rho V^2\right)$, pounds per square foot
R	Reynolds number $\left(\frac{VL}{\nu}\right)$
S_p	engine frontal area, square feet
u	local velocity in boundary layer, feet per second
U	local velocity immediately outside boundary layer, feet per second
V	velocity, feet per second
y	normal distance from surface, inches
α	angle of attack, degrees
ν	kinematic viscosity, feet squared per second
ρ	mass density, slugs per cubic foot

~~CONFIDENTIAL~~

Subscripts

- o free stream
- 1 inlet station (0.10 inch behind lip leading edge)
- 2 diffuser exit
- a settling chamber (rake station)
- E exit station
- 7 local

APPARATUS

Wind Tunnel and Model

The investigation of an NACA submerged inlet at supersonic Mach numbers was performed in the Ames 8- by 8-inch supersonic wind tunnel. The tunnel and its auxiliary equipment are described in reference 7. The test Reynolds number per foot of length was approximately 7 million at the lowest Mach number (1.17) and 11 million at the highest Mach number (1.99).

The model was a 1/4-scale reproduction of the submerged inlet model used in reference 5. A photograph of the model mounted in the wind tunnel is shown in figure 1 and a drawing showing the model dimensions is presented in figure 2. The model was placed outside the influence of the tunnel-wall boundary layer by use of a mounting plate as shown in both figures 1 and 2.

The model was cast from a bismuth and tin alloy, consisting of equal parts by weight, and then was hand worked to the final contour. Both the round- and sharp-lip profiles which were investigated are shown in figure 3. The external surface of the sharp lip was inclined 6° to the free-stream direction. The cross-sectional-area distributions in the diffuser aft of the lip leading edge for both lips are shown in figure 4.

Instrumentation

The model instrumentation is shown in figure 5. Total pressures were measured in the diffuser, approximately at station 7.20, by a

~~CONFIDENTIAL~~

five-tube total-pressure rake. A static orifice measurement which indicated the total pressure at the diffuser wall was also obtained. Each measurement was weighted equally to obtain an average total pressure. Static pressure orifices were located along the ramp center line from station 0.65 to station 5.15 which was 1.25 inches downstream from the lip leading edge. Static orifices were also located along the ramp and body near the intersection with one of the sidewalls.

Boundary-layer profiles were measured on the ramp center line approximately 0.20 inch forward of the lip leading-edge station. Measurements were made with a single probe tube which was adjustable from outside the wind tunnel.

Air flow was induced through the inlet by two constant-speed vacuum pumps. The air passed from the inlet and diffuser into a rotameter outside the wind tunnel where the mass flow was measured. A valve located in the line between the model and the rotameter was used to control the mass flow.

All pressure measurements were recorded photographically from a back-lighted multiple-tube mercury manometer. The flow about the model was observed and photographed through a two-mirror schlieren system.

TEST PROCEDURE

To eliminate the effect of wind-tunnel boundary layer on the test results it was necessary to mount the model away from the tunnel wall. The approximate thickness required for the model mounting plate was determined from a boundary-layer survey made on the wind-tunnel wall at the model nose station. The boundary-layer profile was found to be essentially unchanged over the Mach number range from 1.17 to 1.41 and was assumed to remain unchanged at the higher test Mach numbers. Preliminary measurements of pressure recovery and mass-flow ratio were obtained with the model installed to determine the exact mounting-plate thickness. It was found by testing several plate thicknesses that with a plate thickness 75 percent of the boundary-layer thickness, based on a value of u/U equal to 0.99, the effect of the wind-tunnel boundary layer on the test results appeared to be eliminated. A static pressure needle was attached to the nose of the model for the purpose of determining the exact free-stream Mach number. (See fig. 5.) After the test Mach numbers were determined the needle was removed because separation of the needle boundary layer, due to the body bow wave, affected the inlet performance.

The test Mach numbers were 1.17 and 1.26 for the round-lip configuration and varied from 1.17 to 1.99 for the sharp-lip configuration.

Total-pressure recovery in the model settling chamber (H_3/H_0) and static pressure distribution along the ramp were measured over a range of mass-flow ratios at each Mach number. The range of mass-flow ratios extended from the maximum value for the inlet to a minimum value which was within the region of flow instability. Boundary-layer profiles were measured at one point on the ramp for several representative mass-flow ratios at each Mach number.

The following table indicates the data presented in this report:

M_0	Lip shape	Data presented			
		H_3/H_0	m_1/m_0	Pressure distribution	Boundary-layer profiles
1.17	Round	x	x	- - -	- - -
1.17	Sharp	x	x	x	x
1.26	Round	x	x	- - -	- - -
1.26	Sharp	x	x	- - -	x
1.33	Sharp	x	x	- - -	x
1.41	Sharp	x	x	x	x
1.58	Sharp	x	x	- - -	- - -
1.77	Sharp	x	x	- - -	- - -
1.99	Sharp	x	x	- - -	- - -

RESULTS AND DISCUSSION

Pressure Recovery and Mass-Flow Ratio

Total-pressure-ratio and mass-flow-ratio characteristics of the submerged inlet were obtained for model angles of attack of 0° and 6° . Initial tests were conducted using a round-lip profile and the results are shown in figure 6 for Mach numbers of 1.17 and 1.26. Because the maximum mass-flow ratio and total-pressure ratio were low, further tests were made using a sharp lip in an effort to improve the performance of the inlet. The internal contraction due to the lip shape (see fig. 4) was removed so as to permit attachment of the lip shock wave at low supersonic Mach numbers. Results of these tests are shown in figure 7 for Mach numbers of 1.17 to 1.99 at $\alpha = 0^\circ$ and for Mach numbers of 1.17 to 1.41 at $\alpha = 6^\circ$.

The maximum pressure recovery for both lip shapes at an angle of attack of 0° and a Mach number of 1.17 was approximately 0.83. The maximum mass-flow ratio at these test conditions was 0.83 for the round lip and 0.85 for the sharp lip. Increasing the Mach number to 1.26 for both lip configurations only slightly affected the maximum mass-flow ratio, but reduced the maximum pressure recovery ratio to about 0.80.

Investigation of the sharp lip at Mach numbers above 1.26 showed that the maximum total-pressure ratio continued to decrease with increasing Mach numbers. At the maximum test Mach number, $M_0 = 1.99$, the maximum total-pressure ratio was only 0.52 or about 72 percent of the total-pressure ratio which would occur across a normal shock wave at the same Mach number. The maximum mass-flow ratio remained essentially constant for Mach numbers up to $M_0 = 1.58$. For further increases in Mach number, the maximum mass-flow ratio decreased. Schlieren observations showed a nearly normal shock wave present on the ramp immediately forward of the entrance for all Mach numbers up to $M_0 = 1.58$. At this Mach number the shock wave became attached to the sharp lip at the maximum mass-flow ratio. The entrance Mach number then increased from a subsonic value to a supersonic value greater than M_0 since the flow was accelerated due to the turning angle on the ramp. As a result of these flow conditions at the entrance, increasing the free-stream Mach number above 1.58 caused a decrease in local inlet air density which resulted in a decrease in the maximum mass-flow ratio.

Increasing the angle of attack of the submerged inlet to 6° (figs. 6 and 7) reduced both the pressure recovery and mass-flow ratio at all Mach numbers. The pressure recovery was reduced by about 0.05 and the mass-flow ratio was reduced by 0.03 at the Mach numbers shown in figures 6 and 7. These increments agree qualitatively with those of reference 5 which also utilizes a half body of revolution for the basic body.

Static Pressure and Mach Number Distribution

The distribution of the static pressure coefficient along the ramp center line is shown in figure 8 for the inlet with the sharp lip. The distribution over the basic body in the vicinity of the inlet has been estimated using available characteristic solutions and is also shown. Data are presented for representative mass-flow ratios at Mach numbers of 1.17 and 1.41. The flow is compressed through the bow wave and then, as shown, expands over the nose of the body and continues to expand rapidly along the inlet ramp until, at a station slightly forward of the lip leading edge, a static pressure coefficient is reached which is considerably less than the free-stream value. At this point a nearly normal shock wave occurs at all mass-flow ratios. The exact location of this shock wave is not shown in figure 8 because of an insufficient number of static orifices on that portion of the ramp. For mass-flow ratios less than that for maximum pressure recovery, the shock wave is followed by subsonic compression of the flow inside the diffuser. As the mass-flow ratio is increased above the value for maximum pressure recovery, the flow inside the diffuser re-expands and at the maximum mass-flow ratio again becomes supersonic, as indicated by the value of $P_{critical}$. This supersonic flow terminates in a second normal shock

wave which is also indicated by the rapid decrease in pressure recovery at the maximum mass-flow ratios shown in figure 7. Data which are not presented show the static pressure distribution was relatively unaffected by lip shape; however, the re-expansion inside the diffuser was slightly more rapid when the round lip was used. This was a result of the internal contraction due to the lip curvature. Mention should also be made of the effect of the basic body on the ramp expansion. It is seen in figure 8 that if the inlet were placed at a station on the basic body where the free-stream Mach number exists, the final Mach number to which the flow is expanded on the ramp would be considerably reduced. This expansion due to the basic body will be shown in later discussions to have a considerable adverse effect on inlet performance.

The Mach number distribution along the ramp and into the first portion of the diffuser is shown in figure 9 for the mass-flow ratios giving maximum pressure recovery at free-stream Mach numbers from 1.17 to 1.41. The maximum Mach number on the ramp occurs immediately forward of the ramp shock wave and is considerably higher than the free-stream Mach number. The effect of this flow acceleration on the maximum mass-flow ratio is shown in the table below where the maximum measured mass-flow ratio $(m_1/m_0)_{max}$ is compared to the maximum attainable mass-flow ratio m_0'/m_0 which is based on the maximum ramp Mach number. This quantity, m_0'/m_0 , represents the maximum possible mass-flow ratio which could be obtained if the external-ramp shock wave moved inside the diffuser.

M_0	$\left(\frac{m_1}{m_0}\right)_{max}$	$\frac{m_0'}{m_0}$	$\frac{(m_1/m_0)_{max}}{m_0'/m_0}$
1.17	0.855	0.890	0.961
1.26	.854	.882	.969
1.33	.848	.871	.974
1.41	.866	.869	.997

The values of m_0'/m_0 are considerably less than 1.00 as a result of the expansion on the ramp, and the maximum measured mass-flow ratio varies from 96 to almost 100 percent of this maximum possible value.¹ These results indicate the relative unimportance of mass-flow spillage compared to the flow expansion in reducing the maximum mass-flow ratio of the submerged inlet.

¹The quantity m_1/m_0' approaches 1.00 even though the decrement in mass flow due to the boundary layer was not considered in calculating m_0'/m_0 . This decrement is small and may be balanced by the possible error, ± 2 percent, involved in the calculation.

Boundary Layer

The boundary-layer velocity profiles presented in figure 10 offer a possible explanation for the character of the internal flow behind the lip leading edge. (See fig. 8.) The profiles shown were measured on the ramp center line approximately 0.20 inch forward of the sharp-lip leading edge. The boundary-layer profiles obtained when using the round lip were almost identical to those shown for the sharp lip.

The profiles indicate that the flow at the survey station was almost separated at the lower mass-flow ratios for all Mach numbers shown. Increasing the mass-flow ratio reduced the tendency to separate and all profiles not influenced by separation are almost identical regardless of mass-flow ratio or Mach number. From these characteristics it seems possible that separation actually occurred a short distance downstream of the survey station and moved rearward as the mass-flow ratio was increased. Schlieren photographs show that the external shock wave also moved toward the entrance. Shock-wave interaction with the boundary layer could have caused the onset of separation.

The occurrence of flow separation near the duct entrance could be expected to alter the pressure distribution along the internal duct because the separated region would effectively change the longitudinal distribution of the duct cross-sectional area. With the point of separation well forward of the inlet, the separated region would not reduce the effective duct area distribution in a manner which would disrupt the diffusion process. This was probably the case at low mass-flow ratios and resulted in a steady rise in static pressure with increasing distance downstream of the inlet. (See fig. 8.) At high mass-flow ratios, it is believed that the separation point moved sufficiently close to the inlet to allow the abrupt initial increase in thickness of the separated region to cause a contraction or an effective throat within the diffuser. This throat caused the internal flow to accelerate and become sonic at free-stream Mach numbers below 1.58. In this Mach number range an external shock wave exists and it would be expected that when the internal flow became sonic, the maximum mass-flow ratio was also obtained. At Mach numbers greater than 1.58 the shock wave moved into the diffuser and itself limited the mass-flow ratio.

Although the boundary-layer separation was believed to be the primary factor in establishing the sonic throat, inlet geometry also influenced this condition. The effects of geometric contraction due to the round lip have previously been mentioned. A discontinuity in slope of the ramp surface at the entrance station as shown in figure 2 may also have been a contributing factor.

Comparison With Previous Submerged Inlet Tests

A comparison is shown in figure 11 of the maximum total-pressure recovery as measured in the present investigation (curve A) with similar data from tests of larger scale submerged inlets at transonic speeds. Data for this comparison were taken from references 5 and 6. The maximum test Mach numbers of these investigations approached the minimum Mach number of the present investigation. If the referenced data are extrapolated to a Mach number of 1.17, the pressure recovery of the present submerged inlet at this Mach number is approximately 8 to 10 percent lower than that of the inlets tested at transonic speeds. It is believed that this difference is not excessive when consideration is given to the differences in model scale and shape as well as to the different test conditions. In this regard, it should be mentioned that the pressure recovery shown for reference 5 represents conditions at the entrance to the subsonic diffuser rather than at the exit, as in the case of the present investigation. Under normal subsonic entrance conditions the subsonic diffuser efficiency would be about 0.96, which, when applied to the results of reference 5, would give a pressure recovery of about 0.89 at the diffuser exit. The fact that evidence of boundary-layer separation was obtained in the present investigation but was not shown in reference 5 could account for much of the remaining difference in pressure recovery between the two models. It is believed that separation was prevented in reference 5 because of the lower test Mach number and possibly because of the favorable pressure gradient on the surface of the transonic bump which was used for the investigation.

For the model of reference 6, the duct entrance was located near the body station at which the local Mach number was near that of the free stream, whereas, in the present investigation, the local Mach number at the entrance station on the body was approximately 0.20 greater than the free-stream value. This increase in inlet Mach number due to the body was in addition to that due to the flow expansion on the ramp. As a result, the normal-shock pressure losses were increased, which in turn reduced the total-pressure recovery. A curve which has been corrected for the body effect on the maximum pressure recovery of the present investigation is shown in figure 11. This curve, B, was obtained by transferring the values of maximum pressure recovery, as obtained at the test Mach numbers, to higher Mach numbers approximately equal to those which exist on the basic body at the inlet station. By extrapolating the above curve, good correlation was obtained with the results of reference 6. It is clearly indicated that for minimum losses in pressure recovery and mass-flow ratio the inlet-body combination should be carefully selected to obtain the minimum Mach number at the duct entrance.

All remaining comparisons in this report involve the conditions of curve B which considers the submerged inlet to be located so that the entrance is at the free-stream Mach number station on the basic body.

INLET EVALUATION

To adequately evaluate the performance of the submerged inlet at supersonic Mach numbers, it is essential that its performance be compared with that of an inlet which gives good performance at the lower supersonic Mach numbers where the submerged inlet could be expected to be efficient. A normal-shock scoop inlet located at a position on a body at which the Mach number is that of the free stream has been selected for this comparison.

In figure 11, the maximum pressure recovery calculated for an ideal normal-shock scoop inlet with boundary layer removed is shown for Mach numbers from 1.0 to 2.0 by curve D. This recovery is equal to 96 percent of normal-shock-wave pressure recovery at the free-stream Mach number (the factor of 96 percent is assumed to account for subsonic diffuser efficiency) and is considerably higher than the recovery shown for the submerged inlet, curve B. This difference is a result of the submerged inlet being subjected to the increased losses due to flow expansion on the ramp and the effects of boundary layer. The relative amount of each of these losses is approximated in figure 11 by plotting the estimated maximum pressure recovery for an ideal submerged inlet, curve C. For this curve, 96 percent of the normal-shock pressure recovery at the maximum ramp Mach number is plotted as a function of the free-stream Mach number (inlet station at the free-stream Mach number point on the body). The loss increment between curves D and C then represents the increased shock losses experienced by the submerged inlet because of flow acceleration on the ramp. The effects of the boundary layer on the internal flow of the submerged inlet are believed to account for a large portion of the loss shown between curves C and B. In the lower range of supersonic Mach numbers, the adverse effect of boundary layer on inlet pressure recovery is considerably greater than that which is due to flow acceleration.

To ascertain the over-all performance of the submerged inlet and the normal-shock inlet, net thrust coefficients were calculated for the inlets represented in curves B and D of figure 11, using the method presented in reference 8. This method considers both the thrust and drag of an air-induction system in combination with a propulsive unit. Drag measurements were not obtained in the present investigation; however, the external pressure drag of the submerged inlet was estimated from the pressure distribution measurements on the ramp floor and side walls. The net thrust coefficient C_{FN} , based on A_0 , was computed

as outlined in the appendix of the present report. Similar computations were made for the normal-shock-type scoop inlet, using the data obtained for the open-nose model A of reference 9. The minimum external drag coefficient as measured in the above reference was arbitrarily increased by 50 percent to account for the drag of the boundary-layer gutter which would be necessary in order to make the entrance conditions for a scoop-type inlet comparable to those for an open-nose-type inlet. Limited data available on the drag of such a gutter show this to be a conservative estimate. Since the pressure drag is small for both inlets, however, the accuracy of the estimates is not critical in the final comparison of net thrust coefficients.

In the notation of reference 8, C_{FN}' is a measure of the thermal efficiency of an air-induction system for a given fuel-air ratio. This term can be converted to indicate the relative thrust outputs of different air-induction systems in combination with a given engine if a reference area is used which is unaffected by inlet operation. For this purpose, the net thrust coefficient $(C_{FN})_P$, based on the engine frontal area S_p , was computed for both inlets from the following expression:

$$(C_{FN})_P = C_{FN}' \frac{A_1}{S_p} \frac{m_1}{m_0}$$

The requirement of a fixed corrected weight of air for a given engine relates the inlet areas as follows:

$$\frac{A_{1 \text{ submerged}}}{A_{1 \text{ scoop}}} = \frac{(H_3/H_0)_{\text{submerged}} (m_1/m_0)_{\text{scoop}}}{(H_3/H_0)_{\text{scoop}} (m_1/m_0)_{\text{submerged}}}$$

It must be assumed that the required changes in inlet areas have no appreciable affect on the basic inlet characteristic curves. In figure 12, the net thrust coefficients of the two inlets are compared over a range of similar operating conditions. The comparison is made at Mach numbers of 1.36 and 1.51, using both a turbojet and a turbojet with afterburner. For a turbojet at a Mach number of 1.36, the net thrust coefficient with the submerged inlet is 87 percent of that with the scoop inlet at optimum mass-flow-ratio conditions defined as follows:²

$$\left[\left(\frac{m_1/m_0}{m_1/m_0} \right)_{\text{design}} = 1.00 \right]$$

²The value of $(m_1/m_0)_{\text{design}}$ is taken as the mass-flow ratio for $(C_{FN})_{P_{\text{max}}}$.

Increasing the Mach number to 1.51 reduces this value to 81 percent and further reductions are evident at all mass-flow ratios below the optimum. The comparison is only slightly affected by using a turbojet engine with afterburner in place of the turbojet alone.

CONCLUDING REMARKS

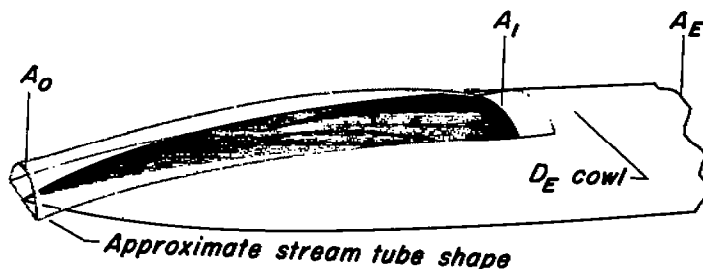
An experimental investigation of an NACA submerged inlet was conducted at Mach numbers from 1.17 to 1.99. A comparison at Mach numbers up to 1.26 showed the effect of lip shape to be small. Maximum total-pressure recovery with the sharp lip decreased from 0.83 at a Mach number of 1.17 to 0.52 at a Mach number of 1.99; however, with an optimum inlet-body combination these values of pressure recovery could be substantially increased.

An evaluation of inlet performance showed that the submerged inlet located at an optimum body position will give a lower net thrust coefficient than an equivalent normal-shock-type scoop inlet at Mach numbers of 1.36 and 1.51.

Ames Aeronautical Laboratory
National Advisory Committee for Aeronautics
Moffett Field, Calif.

APPENDIX

SUBMERGED INLET NET THRUST COEFFICIENT



The net thrust coefficient as defined in reference 8 is

$$C_{FN}' = C_{Fi}' - C_{DE}'$$

or

$$F_N = F_i - D_E \quad (1)$$

Referring to the simplified sketch above and using ΔM to denote a change in total momentum of the entering stream tube,

$$F_i = \Delta M_{O-1} + \Delta M_{1-E} = \Delta M_{O-E} \quad (2)$$

$$D_E = D_{B+S} - D_B + \Delta M_{O-1} \quad (3)$$

The quantity $D_{B+S} - D_B$ is equal to the external pressure and friction drag force due to the air-induction system

$$D_{B+S} - D_B = D_{EO-1} + D_{E1-E}$$

For the submerged inlet assume

$$D_{E1-E} = D_{Ecowl} = 0$$

Then

$$D_{B+S} - D_B = D_{E_{O-1}} = 2D_{E_W} + D_{E_R} \quad (4)$$

The terms D_{E_R} and D_{E_W} are values obtained by integration of the external pressure forces on the ramp and ramp side walls, respectively.

$$D_{E_R} = \int_{\text{ramp L.E.}}^{\text{inlet station}} (p_l - p_o) dA_x$$

$$D_{E_W} = \int_{\text{wall L.E.}}^{\text{inlet station}} (p_l - p_o) dA_x$$

The term ΔM_{O-1} is merely the change in total momentum of the entering stream tube from free-stream conditions to conditions at the inlet and is called scoop incremental drag as suggested in reference 10.³

$$\Delta M_{O-1} = m_1(V_1 - V_o) + (p_1 - p_o) A_1 = D_S \quad (5)$$

Finally

$$D_E = \int_{\text{ramp L.E.}}^{\text{inlet station}} (p_l - p_o) dA_x + 2 \int_{\text{wall L.E.}}^{\text{inlet station}} (p_l - p_o) dA_x + m_1(V_1 - V_o) + (p_1 - p_o) A_1 \quad (6)$$

In coefficient form and using equations 1, 3, 4, and 5,

$$C_{F_N}' = C_{F_1}' - \left(2C_{D_{E_W}} + C_{D_{E_R}} + C_{D_S} \right) \quad (7)$$

The internal thrust coefficient, C_{F_1}' , is dependent upon operating characteristics of the propulsive unit and the total-pressure recovery at the compressor intake. Curves showing the variation of C_{F_1}' over a range of H_3/H_o values at various Mach numbers for altitudes above 35,000 feet are shown in reference 8.

³Further considerations of the stream-tube momentum change forward of the entrance station are extensively discussed in references 11 and 12.

REFERENCES

1. Mossman, Emmet A., Randall, Lauras M.: An Experimental Investigation of the Design Variables for NACA Submerged Entrances. NACA RM A7I30, 1948.
2. Martin, Norman J., and Holzhauser, Curt A.: An Experimental Investigation at Large Scale of Several Configurations of an NACA Submerged Air Intake. NACA RM A8F21, 1948.
3. Hall, Charles F., and Frank, Joseph L.: Ram-Recovery Characteristics of NACA Submerged Inlets at High Subsonic Speeds. NACA RM A8I29, 1948.
4. Axelson, John A., and Taylor, Robert A.: Preliminary Investigation of the Transonic Characteristics of an NACA Submerged Inlet. NACA RM A50C13, 1950.
5. Frank, Joseph L., and Taylor, Robert A.: Comparison of Drag, Pressure Recovery, and Surface Pressure of a Scoop-Type Inlet and an NACA Submerged Inlet at Transonic Speeds. NACA RM A51H20a, 1951.
6. Selna, James, and Schlaff, Bernard A.: An Investigation of the Drag and Pressure Recovery of a Submerged Inlet and a Nose Inlet in the Transonic Flight Range With Free-Fall Models. NACA RM A51H20, 1951.
7. Davis, Wallace F., Brajnikoff, George B., Goldstein, David L., and Spiegel, Joseph M.: An Experimental Investigation at Supersonic Speeds of Annular Duct Inlets Situated in a Region of Appreciable Boundary Layer. NACA RM A7G15, 1947.
8. Brajnikoff, George B.: Method and Graphs for the Evaluation of Air Induction Systems. NACA TN 2697, 1952.
9. Brajnikoff, George B., and Rogers, Arthur W.: Characteristics of Four Nose Inlets as Measured at Mach Numbers Between 1.4 and 2.0. NACA RM A51C12, 1951.
10. Klein, Harold: The Calculation of the Scoop Drag for a General Configuration in a Supersonic Stream. Rep. SM-13744, Douglas Aircraft Co., Inc., April 12, 1950.

11. Sibulkin, Marwin: Theoretical and Experimental Investigation of Additive Drag. NACA RM E51B13, 1951.
12. Wyatt, DeMarquis D.: Aerodynamic Forces Associated with Inlets of Turbojet Installations. Aero. Engr. Review, Oct. 1951, pp. 20-23.

[REDACTED]

NACA RM A52F17

[REDACTED]

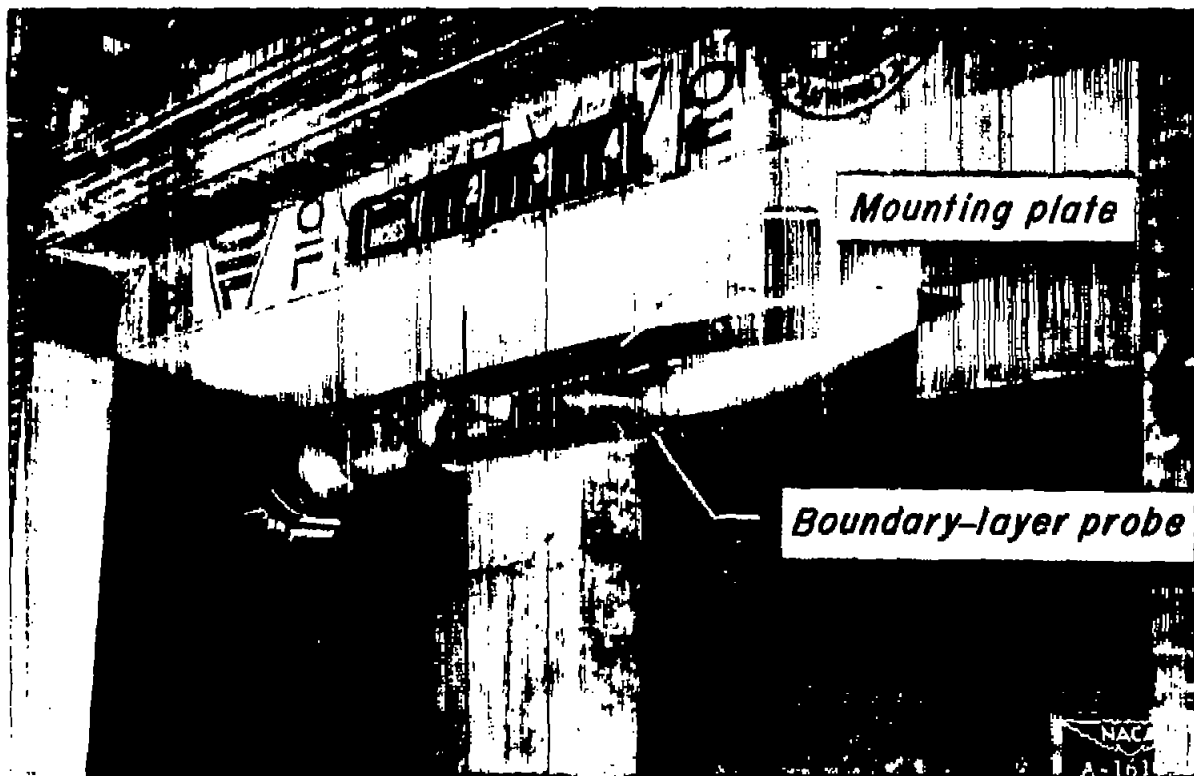
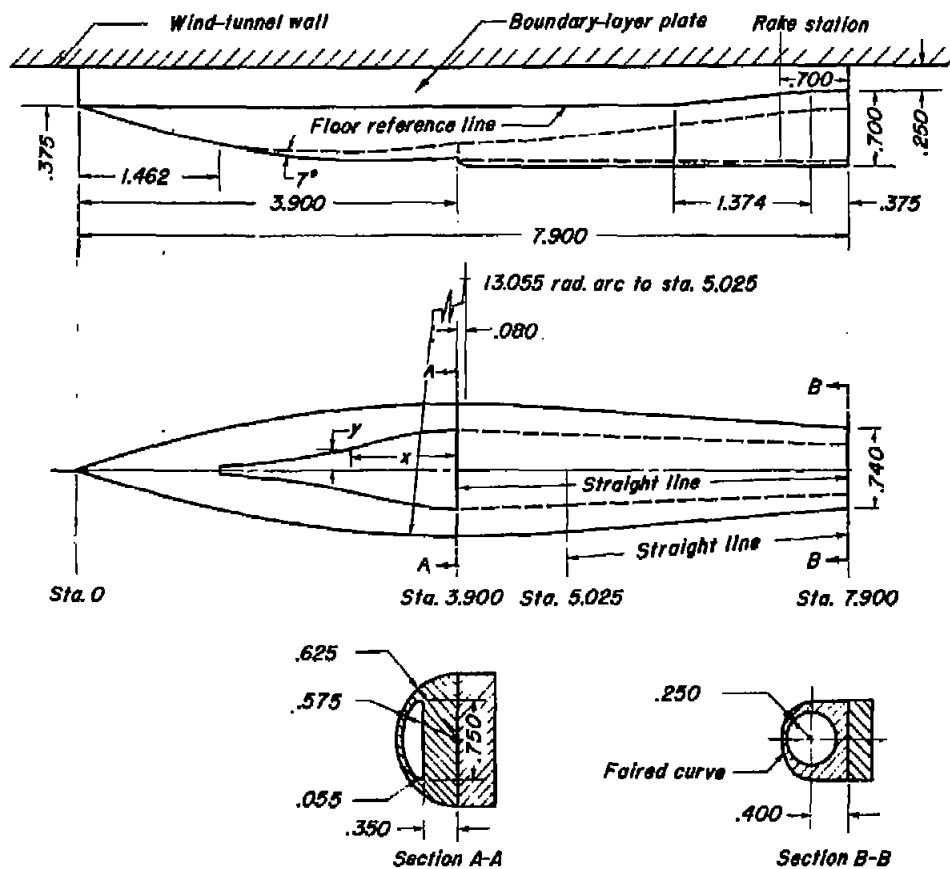


Figure 1.- Photograph of NACA submerged-inlet model mounted on the top wall of the Ames 8- by 8-inch supersonic wind tunnel.

Ramp-floor coordinates		Ramp-wall coordinates	
Sta.	Ord.	x	y
1.462	0.380	0	0.375
1.650	0.407	0.244	0.373
1.900	0.432	0.487	0.343
2.150	0.442	0.731	0.287
2.400	0.442	0.975	0.227
2.650	0.437	1.219	0.181
2.900	0.427	1.462	0.147
3.150	0.417	1.706	0.116
3.400	0.395	1.950	0.088
3.650	0.375	2.194	0.060
3.900	0.350	2.437	0.032

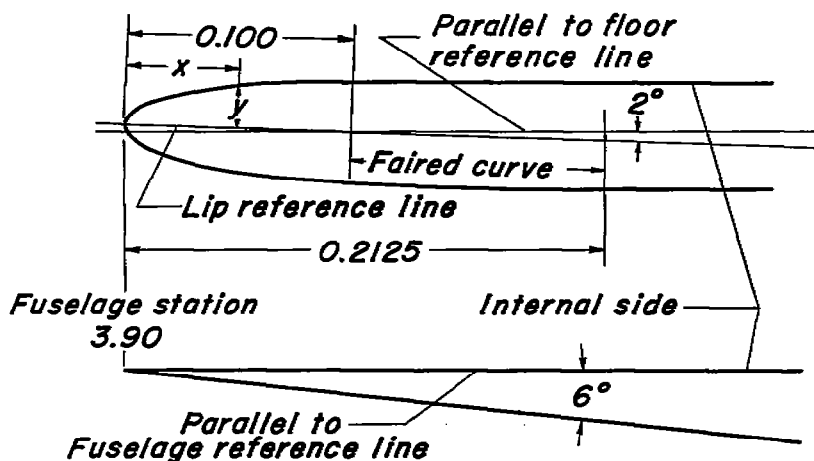
Duct-floor coordinates			
Sta.	Ord.	Sta.	Ord.
3.900	0.350	6.150	0.179
4.150	0.345	6.400	0.149
4.400	0.337	6.650	0.128
4.650	0.327	6.900	0.093
4.900	0.312	7.337	0.041
5.150	0.295	7.400	0.035
5.400	0.266	7.650	0.025
5.650	0.237	7.900	0.025
5.900	0.208		



Note: All dimensions in inches unless otherwise noted.



Figure 2.- Submerged-inlet model.



Round-lip coordinates

x	y	x	y
0	0	.0625	.0222
.0125	.0117	.0750	.0230
.0250	.0160	.0850	.0232
.0375	.0190	.1000	.0235
.0500	.0210		

All dimensions in inches

L.E. radius 0.0092



Figure 3.- Details of round-and sharp-lip profiles.

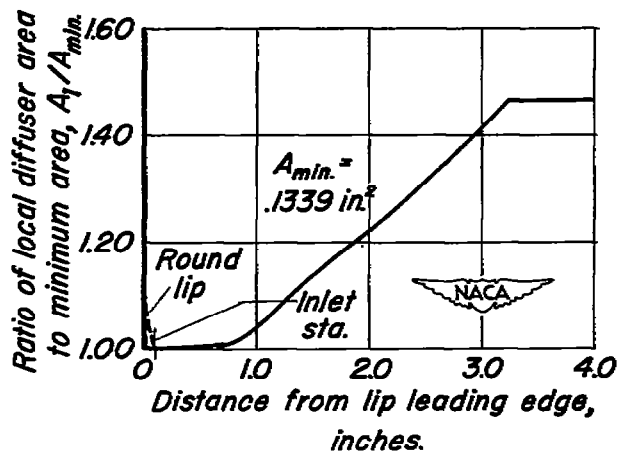


Figure 4.- Cross-sectional-area distribution in diffuser behind lip leading edge.

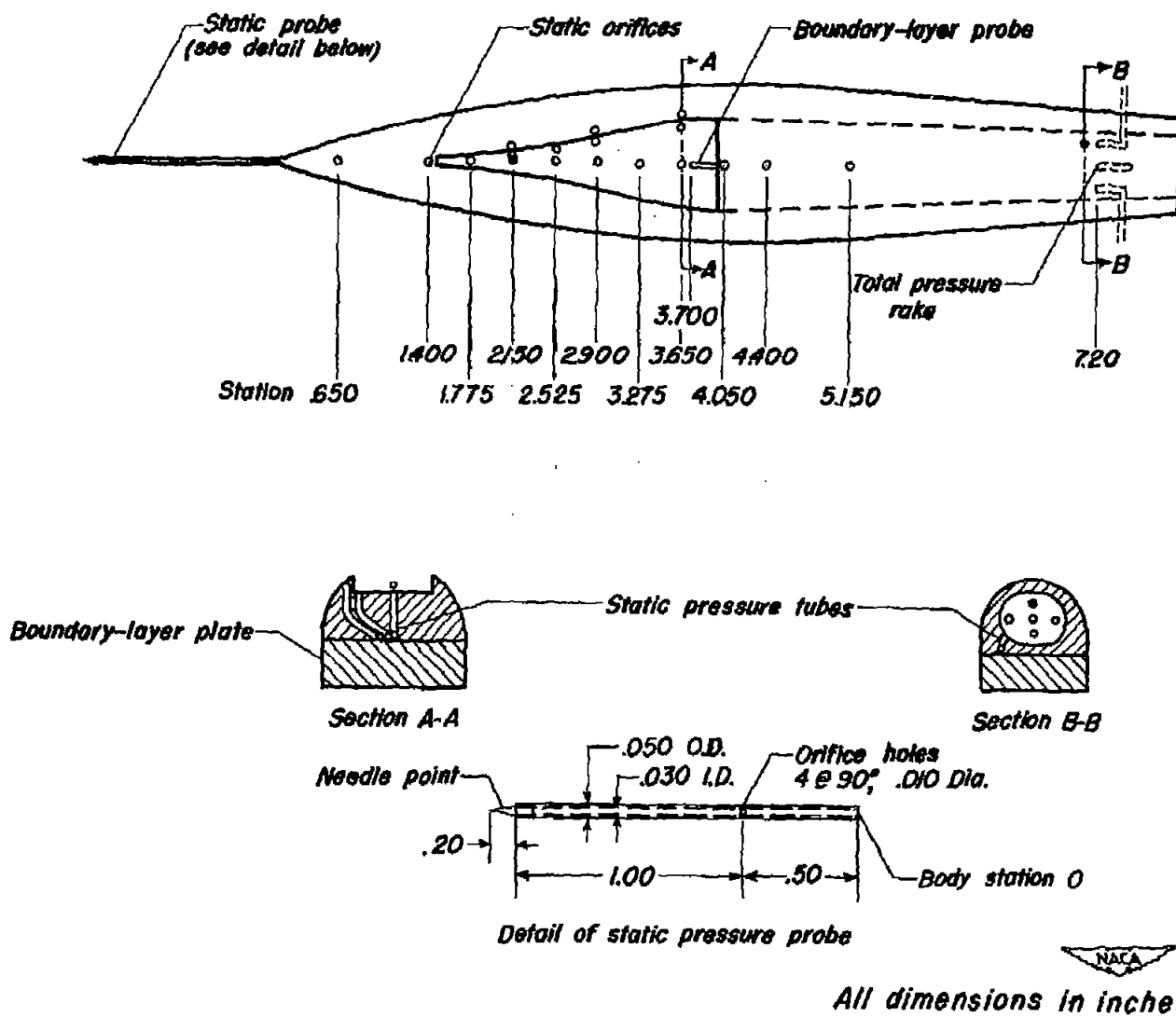


Figure 5. — Instrumentation of submerged inlet model.

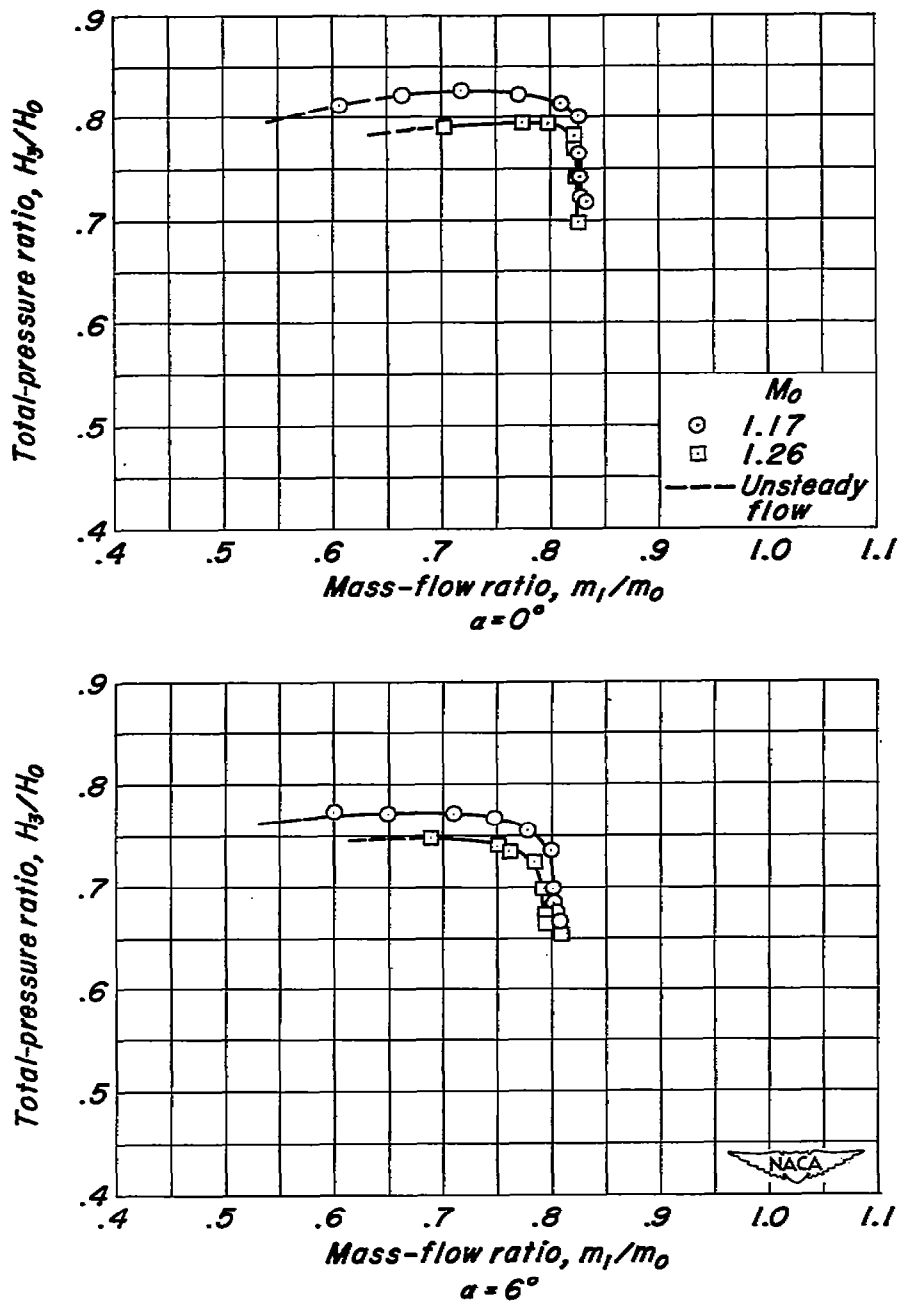


Figure 6.- Variation of total-pressure ratio with mass-flow ratio for a submerged inlet with round lip.

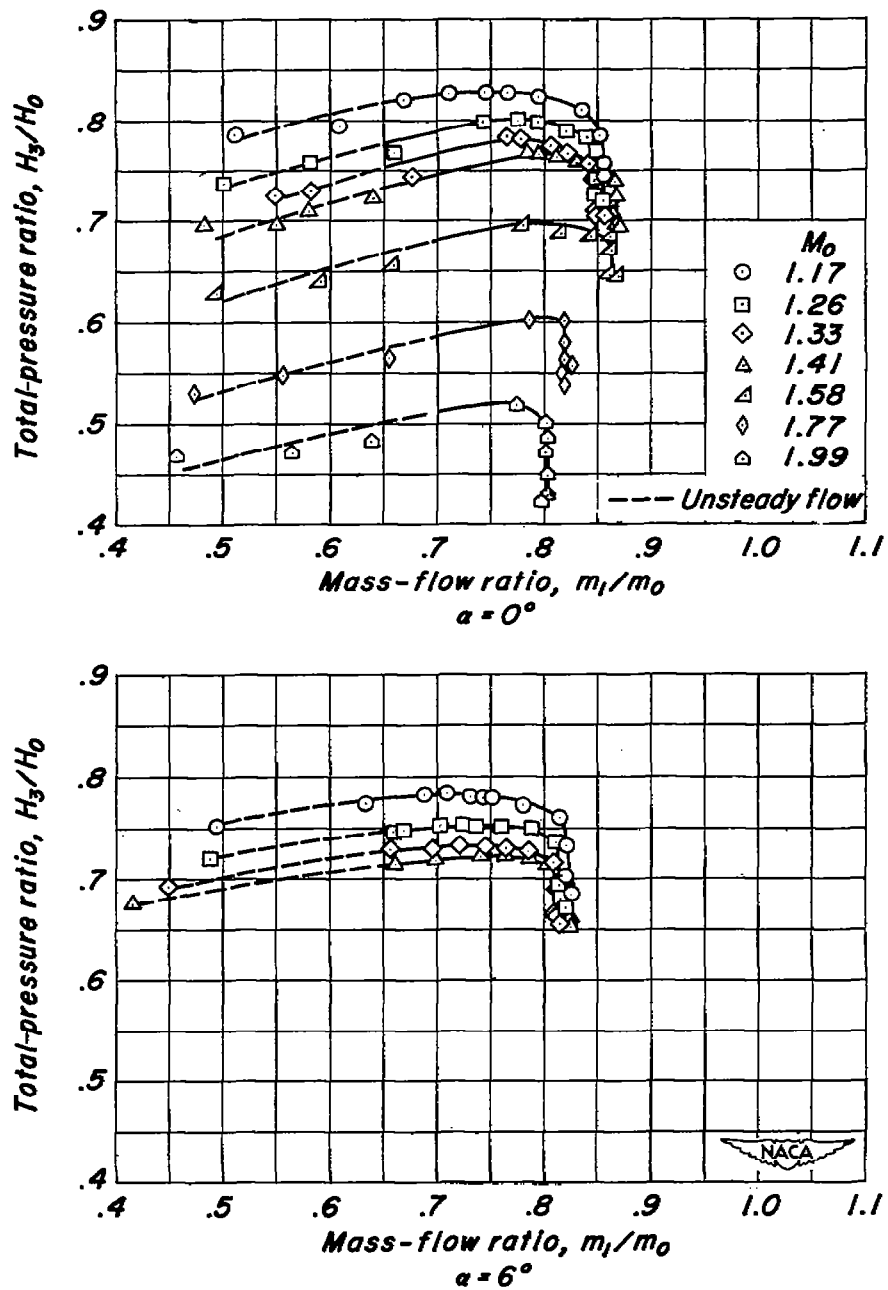


Figure 7.—Variation of total-pressure ratio with mass-flow ratio for a submerged inlet with sharp lip.

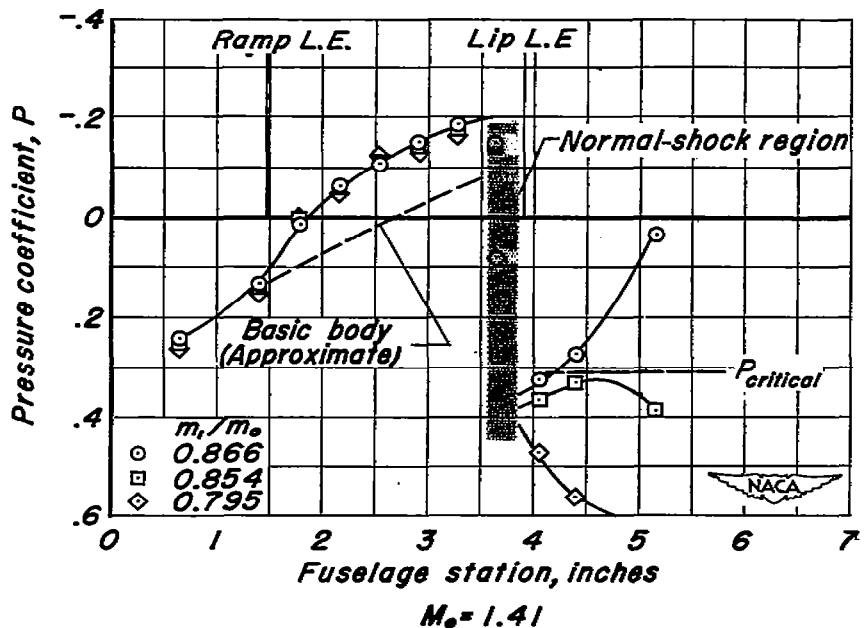
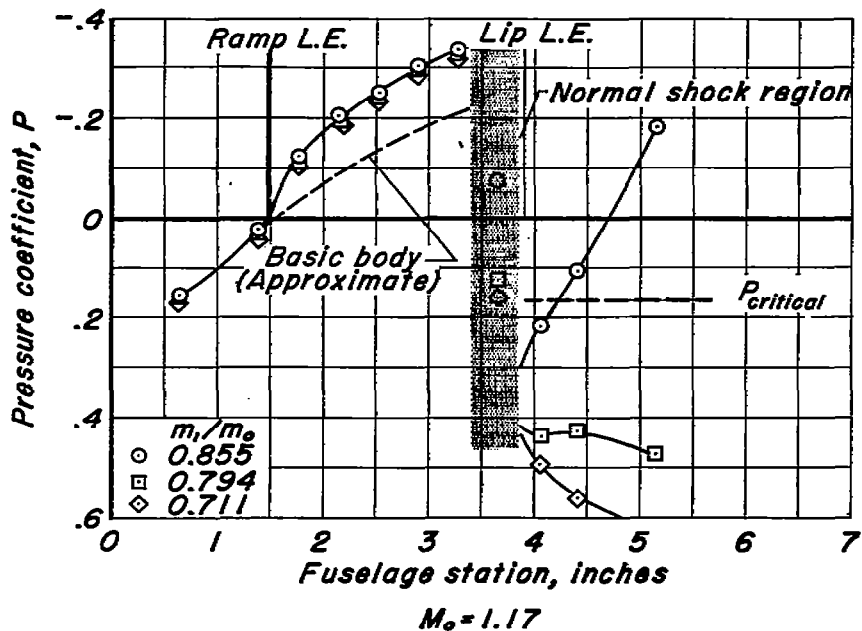


Figure 8.—Variation of pressure coefficient along ramp and duct center line with mass-flow ratio for a submerged inlet with sharp lip. $\alpha = 0^\circ$.

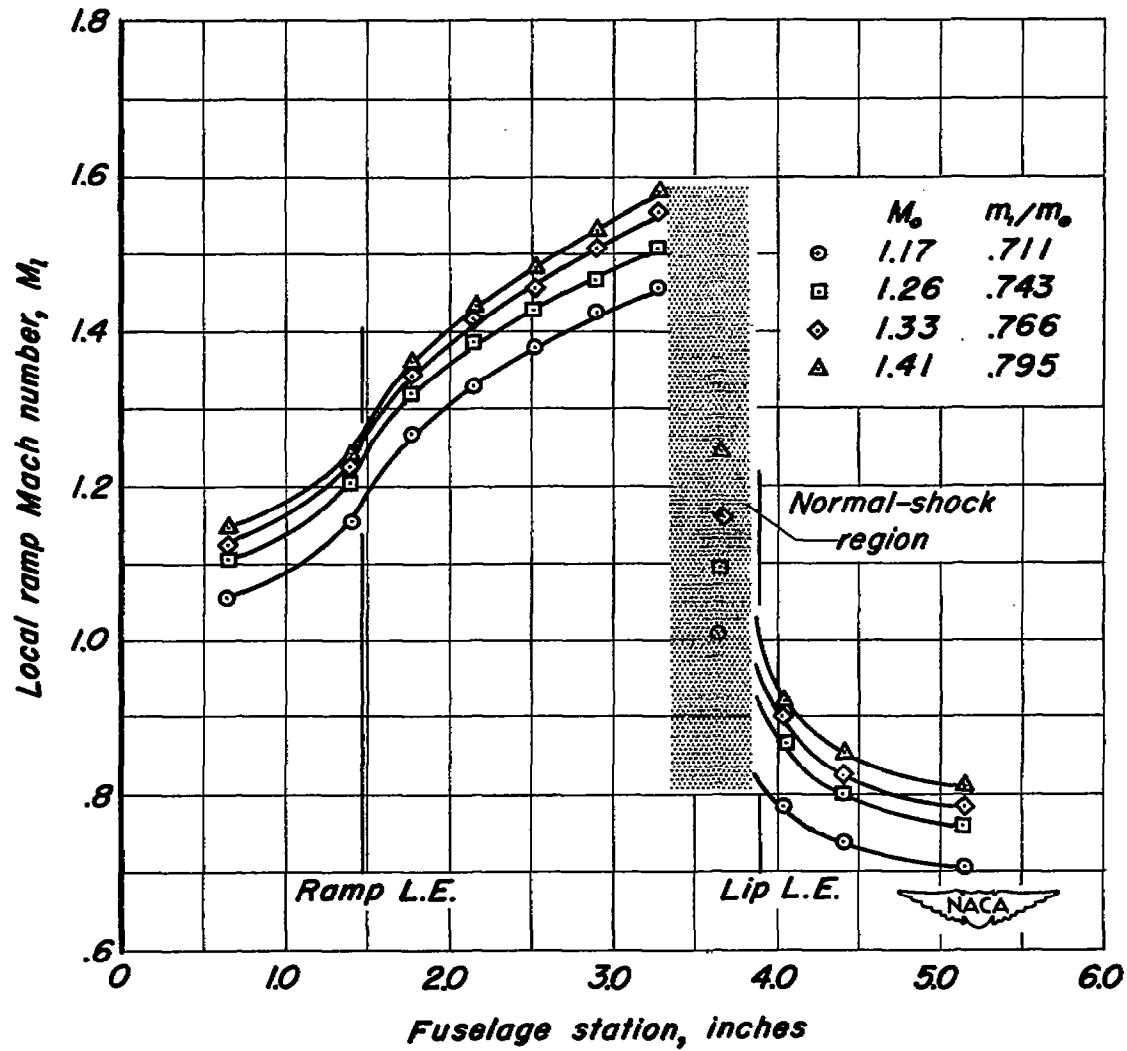


Figure 9.— Variation of local Mach number along ramp center line for several free-stream Mach numbers at maximum pressure recovery. Sharp lip, $\alpha=0^\circ$.

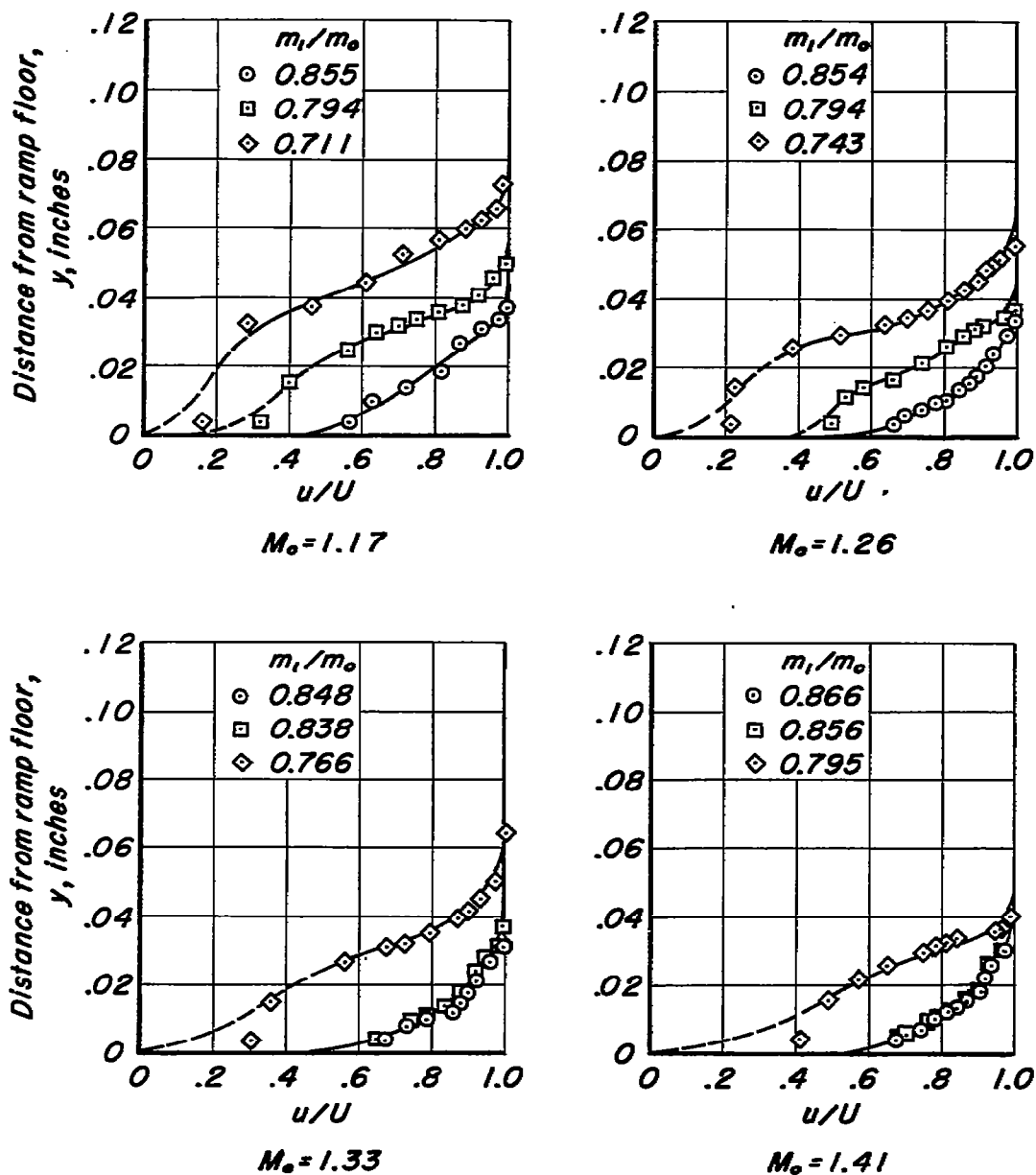


Figure 10.—Variation with mass-flow ratio of boundary-layer profile on ramp center line slightly forward of lip leading-edge station. Sharp lip, $\alpha = 0^\circ$.

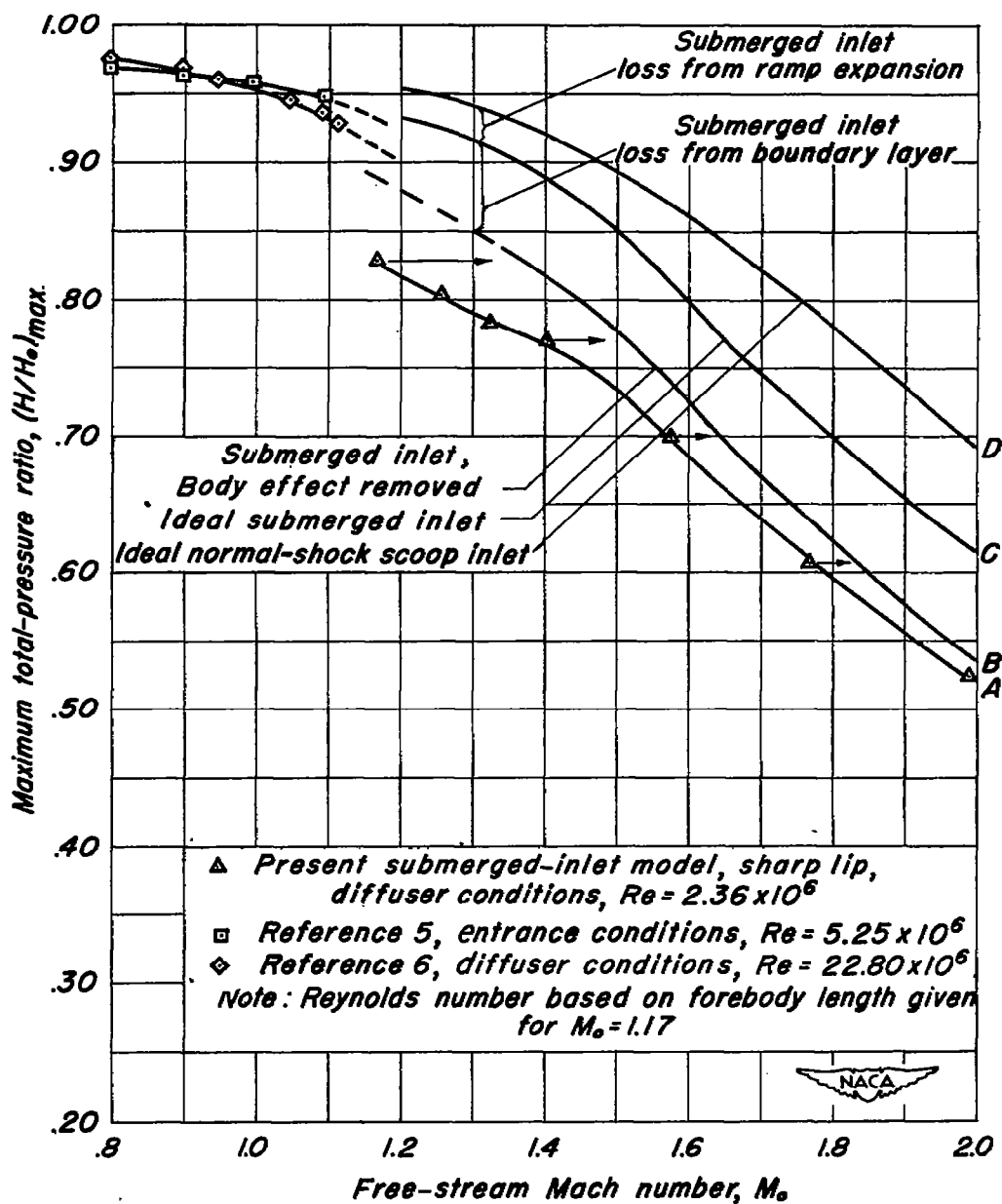


Figure 11.- A comparison of the variation of maximum pressure recovery with Mach number for several submerged inlets and an ideal normal-shock inlet.

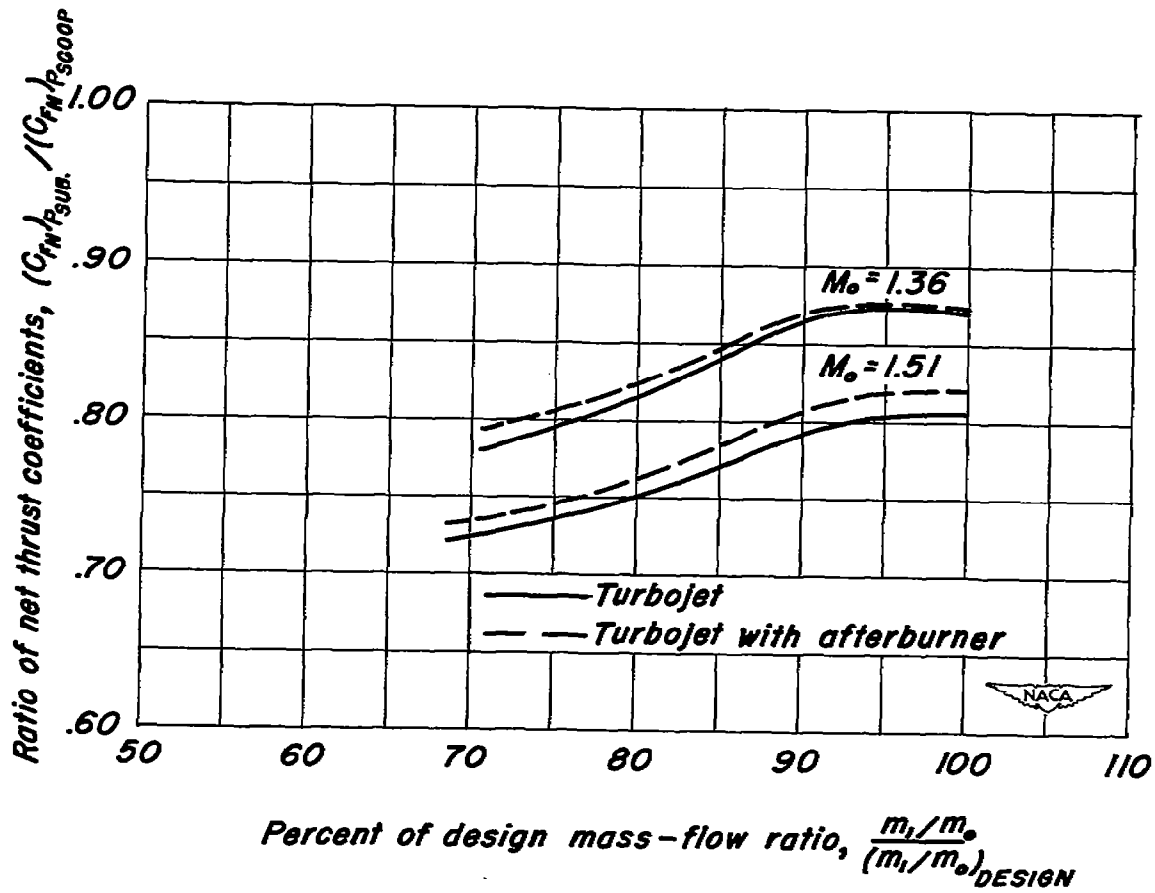
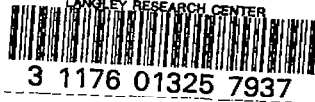


Figure 12.- Variation of the ratio of net thrust coefficients with inlet operating conditions.

SECURITY INFORMATION



DO NOT REMOVE SLIP FROM MATERIAL

Delete your name from this slip when returning material to the library.

NAME	MS
ke	280

NASA Langley (Rev. May 1988)

RIAD N-75

